

Tunability of notch angles in quantum cascade microlasers with highly deformed spiral resonators

Dongxia Qu,^{1,a)} Richard Cendejas,¹ Zhijun Liu,¹ Claire Gmachl,¹ and Fred Towner²

¹Department of Electrical Engineering, MIRTHE, and PRISM, Princeton University, Princeton, New Jersey 08544, USA

²Maxion Technologies, Inc., College Park, Maryland 20740, USA

(Received 13 August 2008; accepted 2 December 2008; published online 31 December 2008)

We study the mode spectra and lasing thresholds of spiral-shaped quantum cascade lasers with a deformation in the range of 10%–45% with respect to the radius and with various notch angles. We observe that the initial lasing wavelength and the threshold of a laser are correlated with each other, and they can be jointly tuned by both the deformation coefficient and notch angle. The dependence of the cavity loss on the deformation coefficient is analyzed via the measured lasing thresholds and frequency dependent gain coefficients. Moreover, we achieve single mode emission by tuning the notch angle and deformation coefficients. © 2008 American Institute of Physics. [DOI: 10.1063/1.3058679]

Microcavity lasers have attracted much attention due to their potential applications in photonic integrated circuits, optical communication systems, and chemical sensors.¹ In 2003, spiral-shaped microcavity lasers were introduced by Chern *et al.*² as an alternative cavity design to achieve unidirectional emission. Since then, spiral-shaped microcavity lasers have been realized with a variety of active media, such as polymers^{3–5} and semiconductors.^{6–8} The emission mechanism of spiral-shaped lasers is interpreted as the diffraction of the propagating whispering gallery modes at the notch.^{9,10} Recently, spiral-shaped quantum cascade (QC) lasers were studied showing single mode emission with zero notch angles and small deformations.⁷

Since emission from a spiral microcavity laser is from the notch, we infer that varying the notch angle may provide an additional degree of freedom in light control. Until now, spiral-shaped QC lasers have only been studied with zero notch angles and a small deformation coefficient of around 0.2.⁷ In this letter, we study the lasing mode characteristics of spiral-shaped QC lasers with high deformations and various notch angles. We observe that the initial lasing frequency and the lasing threshold can be tuned by both the notch angle and the deformation coefficient.

The QC laser structures are grown by molecular beam epitaxy on a low-doped InP substrate. Details of the active regions are described in Ref. 11. Thirty periods of active regions are inserted between two waveguide layers of GaInAs, 400-nm-thick on top and 600-nm-thick at the bottom, both doped to $n_{\text{Si}} \sim 5 \times 10^{16} \text{ cm}^{-3}$. The upper cladding comprises of a 1.5- μm -thick AlInAs layer ($n_{\text{Si}} \sim 1 \times 10^{17} \text{ cm}^{-3}$), followed by a 1.1- μm -thick AlInAs layer ($n_{\text{Si}} \sim 2 \times 10^{17} \text{ cm}^{-3}$). The waveguide structure is completed with a 360-nm-thick GaInAs layer highly doped with $n_{\text{Si}} \sim 8 \times 10^{18} \text{ cm}^{-3}$. The laser is designed to emit light of wavelength $\lambda = 8.5 \mu\text{m}$. The geometry of the spiral laser in polar coordinates is defined as $r(\phi) = r_0[1 + (\epsilon/2\pi)\phi]$, $0 \leq \phi \leq 2\pi - \phi_0$, where r_0 is the radius at $\phi = 0$, ϵ is the deformation coefficient, and ϕ_0 represents the notch angle. The configuration of a spiral-shaped QC laser with $\epsilon = 0.4$ and $\phi_0 = 15^\circ$ is

shown in Fig. 1(a). We use the improved wet-chemical etching technique¹² to fabricate the deep-etched spiral lasers. A SiN/photoresist double layer is used as the mask to etch the semiconductor with a cavity height of 20 μm . After cleaning and spin coating fresh photoresist, the SiN sacrificial layer is etched away by 10:1 buffered oxide etch, leaving the cavity top surface exposed. The top metal contact (Ti/Au, 25 nm/300 nm) is then deposited, followed by lift-off. In this way, the top metal covers the entire top of the resonator, allowing maximum overlap with the propagating modes in the resonator. The sample substrate is coated with Ge/Au (20 nm/300 nm) back contact, soldered on a copper block with indium, and wire bonded as shown in Fig. 1(b).

The lasers are operated in pulsed mode at 80 K with a pulse width of 50 ns and a repetition rate of 78.6 kHz. The maximum pulsed operating temperature of the lasers is 260 K. Our lasers are characterized with ϵ up to 0.45, with r_0 fixed at 63 μm . As a result, the expected lasing resonances are in the range of $140 < nkR < 180$, where n is the refractive index, k is the vacuum wave number, and R is the average cavity radius. For each deformation, the lasers are fabricated with five notch angles: $\phi_0 = 0^\circ, 8^\circ, 15^\circ, 23^\circ, \text{ and } 32^\circ$.

We first investigate the lasers with a fixed deformation but with various notch angles by measuring the laser spectra using a Fourier transform infrared spectrometer equipped with a liquid nitrogen-cooled mercury cadmium telluride detector. Figure 2 shows the measured electroluminescence

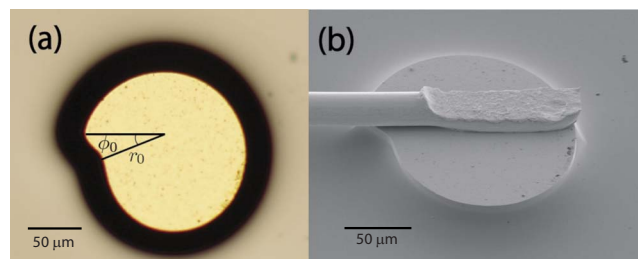


FIG. 1. (Color online) (a) The top-view optical microscope image of a fabricated spiral laser with $\epsilon = 0.4$ and $\phi_0 = 15^\circ$. (b) The side-view scanning electron microscope image of the same laser shown in (a) after wire bonding.

^{a)}Electronic mail: dqu@princeton.edu.

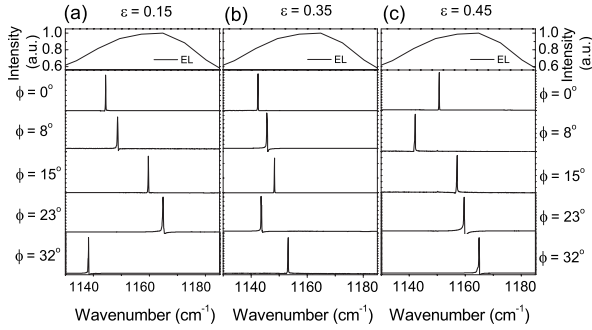


FIG. 2. The measured EL and initial lasing spectra for lasers with (a) $\epsilon=0.15$, (b) $\epsilon=0.35$, and (c) $\epsilon=0.45$ with five different ϕ_0 .

(EL) gain spectra and the initial lasing spectra of lasers with $\epsilon=0.15, 0.35$, and 0.45 and five different notch angles $\phi_0=0^\circ, 8^\circ, 15^\circ, 23^\circ$, and 32° when injection currents are close to the threshold of each device. As the notch angle increases, the initial lasing wavelength moves within the gain spectrum. For example, when ϕ_0 changes from 23° to 32° for lasers with $\epsilon=0.15$, the initial lasing wavelength moves 27 cm^{-1} , about three times the whispering gallery mode spacing (8 cm^{-1}) in a circular resonator with a radius of $63 \mu\text{m}$. For ($\epsilon=0.15, \phi_0=0^\circ$), ($\epsilon=0.15, \phi_0=32^\circ$), and ($\epsilon=0.35, \phi_0=32^\circ$), the initial lasing modes are more than 10 cm^{-1} away from the peak gain at 1162 cm^{-1} . Since the modes away from the peak gain are less amplified, the fact that they lase first suggests they have lower loss than the neighboring modes closer to the gain maximum. Moreover, for injection currents much larger than the threshold, we present the mode spectra for five lasers with ϵ ranging from 0.1 to 0.45 and $\phi_0=8^\circ$, as shown in Fig. 3. For most deformations, the mode spacing is around 8 cm^{-1} . While for ($\epsilon=0.35, \phi_0=8^\circ$), we observe several lasing peaks that do not show well defined mode spacings. This observation may be due to the excitation of higher order transverse modes under the high injection current.

We further characterize the thresholds of the lasers with fixed deformations but with various notch angles. Figure 4 shows the initial lasing wavelength and threshold versus notch angle for three sets of devices with different deformations. We observe that the spectral variation in the initial lasing mode (square) correlates with the variation in the lasing threshold (dot). For most lasers, when the initial lasing mode is closer to the gain peak ($8.6 \mu\text{m}$), the laser has a

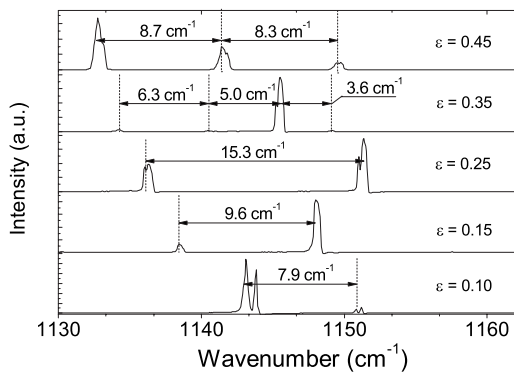


FIG. 3. Spectra of five lasers with the same notch angle, $\phi_0=8^\circ$, and different ϵ , measured with pulsed peak currents of 1.42, 1.50, 1.45, 1.65, and 1.0 A for lasers with $\epsilon=0.1, 0.15, 0.25, 0.35$, and 0.45 , respectively.

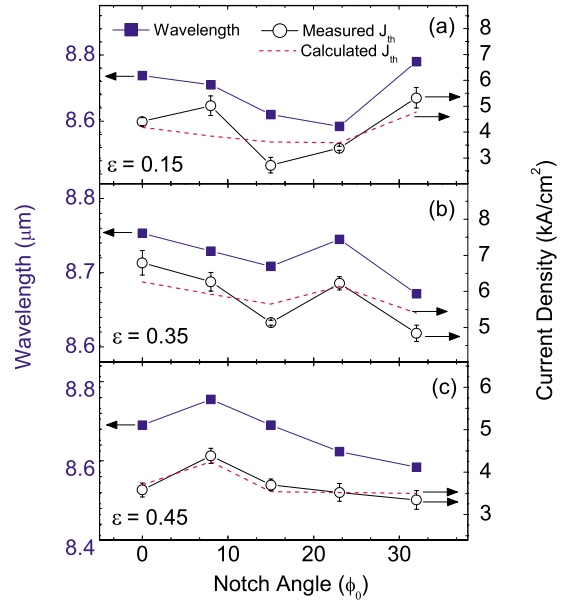


FIG. 4. (Color online) The measured initial lasing wavelengths, measured thresholds, and calculated thresholds of lasers with (a) $\epsilon=0.15$, (b) $\epsilon=0.35$, and (c) $\epsilon=0.45$ with various notch angles.

lower threshold. We calculate the threshold of our lasers by using the following equation:

$$J_{th} = (\alpha_{wav} + \alpha_{out})/g_{\Gamma}(\nu), \tag{1}$$

where J_{th} is the threshold current density, g_{Γ} is the wavelength (frequency) dependent modal gain coefficient, α_{wav} is the material loss, and α_{out} is the outcoupling loss. In particular, α_{wav} depends on the deformation ϵ , notch angle ϕ_0 , the effective refractive index, the area of the resonator, and any scattering from the cavity sidewall. The peak gain coefficient $g_{\Gamma}(\nu_0)$ is calculated to be 10 cm/kA from the laser structure, where ν_0 is the maximum gain frequency.¹³ Through the measured EL gain spectra, we are able to obtain the modal gain coefficient at a specific wavenumber. If $\alpha_{wav} + \alpha_{out}$ is constant for lasers with the same deformation but with different notch angles, we can easily calculate the threshold of lasers with respect to their initial lasing wavelengths. The results are plotted in red dashed lines in Fig. 4, where the overall loss $\alpha_{wav} + \alpha_{out}$ is calculated through the average lasing threshold at each deformation as $36.0, 52.5$, and 34.9 cm^{-1} for $\epsilon=0.15, 0.35$, and 0.45 , respectively. For lasers with $\epsilon=0.15$ and 0.35 , the degree of the measured threshold variation is larger than that predicted by assuming a constant loss for different notch angles. It suggests that in fact a small variation in the notch angle can significantly tune the mode loss, resulting in a threshold variation as large as 1.95 kA/cm^2 .

The dependence of J_{th} on the deformation is also analyzed. Figures 5(a)–5(c) show the measured initial lasing wavelengths, average overall loss, and measured and calculated lasing thresholds as a function of the deformation at three representative notch angles $\phi_0=0^\circ, 15^\circ$, and 23° . The J_{th} (dashed red line) is calculated by including the variation in the gain due to the initial lasing wavelength shifts and assuming a constant overall loss $\alpha_{wav} + \alpha_{out}$ for different deformations. By comparing the measured thresholds with the calculations, we can tell whether the variation in the lasing threshold is from the loss or from the wavelength dependent

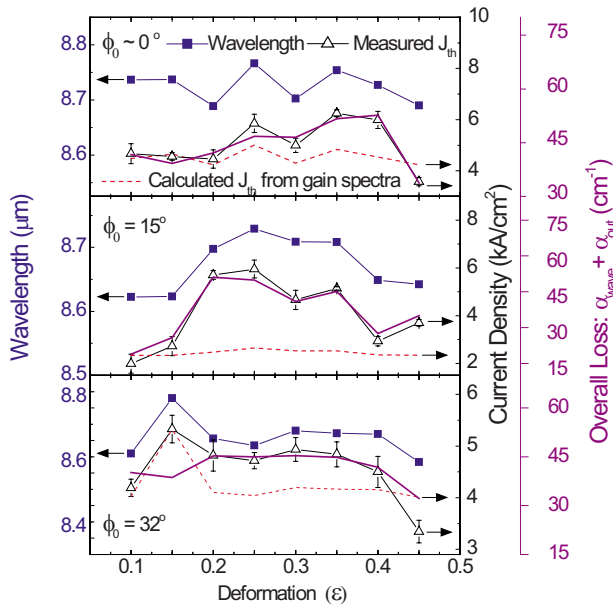


FIG. 5. (Color online) The measured initial lasing wavelengths, measured thresholds, average overall loss $\alpha_{\text{wav}} + \alpha_{\text{out}}$ (without error bars), and calculated thresholds of lasers with (a) $\phi_0 = 0^\circ$, (b) $\phi_0 = 15^\circ$, and (c) $\phi_0 = 32^\circ$ with various deformation factors.

gain. For example, for $(\epsilon = 0.15, \phi_0 = 32^\circ)$, the measured lasing threshold agrees with the calculated value. While for $(\epsilon = 0.2, \phi_0 = 15^\circ)$, the observed lasing threshold is much larger than the predicted value, implying that the increase in the threshold is from the increase in the cavity loss. Hence, we plot the average overall loss (solid line) calculated from Eq. (1) by using the measured J_{th} and frequency dependent modal gain coefficient. With the same cavity radius r_0 , the cavity loss does not monotonically increase with increasing deformation. For three notch angles, at medium deformations ($0.2 \leq \epsilon < 0.4$), the cavity loss increases, while at larger deformations ($0.4 \leq \epsilon \leq 0.45$), the cavity loss becomes smaller. Whether the cavity loss continues to drop for larger deformations ($\epsilon \geq 0.5$) needs further study. The decrease in the cavity loss at some large deformations could be due to the suppression of the light leakage, which results from the resonant interference between the propagating waves supported by the cavity.¹⁴ Furthermore, the Q factor of our lasers is estimated as $Q = (2\pi n) / (\lambda J_{\text{th}} g_{\text{T}})$, where $n = 3.2$ is the effective refractive index and λ is the wavelength. From the experimentally measured J_{th} ranging from 1.14 to 6.79 kA/cm², the Q factor of our lasers is estimated to be from 300 to 2000.

We observe single mode emission in spiral QC lasers with both small and medium deformations. Figures 6(a) and 6(b) plot the log-scale spectra of the selected lasers with $(\epsilon = 0.35, \phi_0 = 15^\circ)$ and $(\epsilon = 0.35, \phi_0 = 23^\circ)$. Both lasers show single mode emission with a maximum side mode suppression ratio of ~ 30 dB. The laser with $\phi_0 = 15^\circ$ supports single mode emission from the lasing threshold (0.75 A) to 1.34 A. With a larger notch angle, i.e., $\phi_0 = 23^\circ$, the laser exhibits single mode emission with an injection current ranging from the threshold (0.85 A) to 1.30 A. Further optimizing the cav-

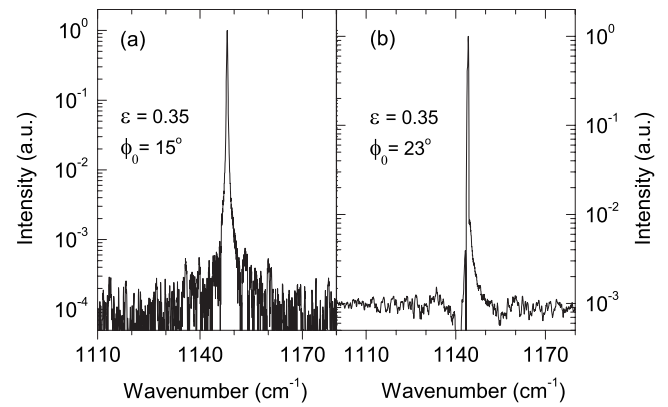


FIG. 6. Single mode spectra plotted in a logarithmic scale for the two QC lasers with parameters (a) $\epsilon = 0.35, \phi_0 = 15^\circ$ with a peak current of 1.34 A and (b) $\epsilon = 0.35, \phi_0 = 23^\circ$ with a peak current of 1.27 A.

ity shape to support single mode emission with a lower lasing threshold is interesting for future study.

In conclusion, we have tested spiral-shaped QC lasers with a deformation up to 0.45 and five-notch angles. The laser performance is jointly tuned by the interplay of wavelength dependent gain, large free spectral range of the micro-cavity laser, and the loss from deformations and notch angles. Counterintuitively, the cavity loss becomes smaller at certain large deformations. Further optimization of the cavity shape to ensure a match between the initial lasing wavelength and the gain peak is essential for future study to make a single mode spiral-shaped QC laser with a low lasing threshold.

The authors would like to thank Grace D. Chern Metcalfe in the U. S. Army Research Laboratory for helpful discussion. This work was supported in part by MIRTHER (NSF-ERC).

- ¹F. Vollmer, D. Braun, A. Libchaber, M. Khoshshima, I. Teraoka, and S. Arnold, *Appl. Phys. Lett.* **80**, 4057 (2002).
- ²G. D. Chern, H. E. Tureci, A. D. Stone, R. K. Chang, M. Kneissl, and N. M. Johnson, *Appl. Phys. Lett.* **83**, 1710 (2003).
- ³T. Ben-Messaoud and J. Zyss, *Appl. Phys. Lett.* **86**, 241110 (2005).
- ⁴A. Fujii, T. Takashima, N. Tsujimoto, T. Nakao, Y. Yoshida, and M. Ozaki, *Jpn. J. Appl. Phys., Part 2* **45**, L833 (2006).
- ⁵A. Tulek and Z. V. Vardeny, *Appl. Phys. Lett.* **90**, 161106 (2007).
- ⁶M. Kneissl, M. Teepe, N. Miyashita, N. M. Johnson, G. D. Chern, and R. K. Chang, *Appl. Phys. Lett.* **84**, 2485 (2004).
- ⁷R. Audet, M. A. Belkin, J. A. Fan, B. G. Lee, K. Lin, F. Capasso, E. E. Narimanov, D. Bour, S. Corzine, J. Zhu, and G. Hoffer, *Appl. Phys. Lett.* **91**, 131106 (2007).
- ⁸C.-M. Kim, J. Cho, J. Lee, S. Rim, S. H. Lee, K. R. Oh, and J. H. Kim, *Appl. Phys. Lett.* **92**, 131110 (2008).
- ⁹F. Courvoisier, V. Boutou, J. P. Wolf, R. K. Chang, and J. Zyss, *Opt. Lett.* **30**, 738 (2005).
- ¹⁰T. Kwon, S. Lee, M. S. Kurdoglyan, S. Rim, C. Kim, and Y. Park, *Opt. Lett.* **31**, 1250 (2006).
- ¹¹C. Gmachl, F. Capasso, J. Faist, A. L. Hutchinson, A. Tredicucci, D. L. Sivco, J. N. Baillargeon, S. N. G. Chu, and A. Y. Cho, *Appl. Phys. Lett.* **72**, 1430 (1998).
- ¹²R. Colombelli, C. Gmachl, A. M. Sergent, D. L. Sivco, E. E. Narimanov, V. A. Podolskiy, A. Y. Cho, and F. Capasso, *IEEE J. Sel. Top. Quantum Electron.* **12**, 66 (2006).
- ¹³C. Gmachl, F. Capasso, E. E. Narimanov, J. U. Nöckel, A. D. Stone, J. Faist, D. L. Sivco, and A. Y. Cho, *Science* **280**, 1556 (1998).
- ¹⁴W. Fang, A. Yamilov, and H. Cao, *Phys. Rev. A* **72**, 023815 (2005).